This manuscript is published in MRS Advance, which can be cited as,
S. I. Hossain, Neha S. Gandhi, Zak E. Hughes, Suvash C. Saha, Computational Modelling of the Interaction of Gold Nanoparticle with Lung Surfactant Monolayer, *MRS Advances*, 4 (20), 1177-1185, 2019. doi.org/10.1557/adv.2019.93

Computational Modelling of the Interaction of Gold Nanoparticle with Lung Surfactant Monolayer

Sheikh I. Hossain[1], Neha S. Gandhi[2], Zak E. Hughes[3], Suvash C. Saha[1]

[1]*School of Mechanical and Mechatronic Engineering, University of Technology Sydney, 81 Broadway, Ultimo NSW 2007, Australia*

[2]*School of Mathematical Sciences, Queensland University of Technology, 2 George Street, GPO Box 2434, Brisbane QLD 4001,*

[3]*School of Chemistry and Biosciences, The University of Bradford, Bradford, BD7 1 DP, UK*

ABSTRACT

Lung surfactant (LS), a thin layer of phospholipids and proteins inside the alveolus of the lung is the first biological barrier to inhaled nanoparticles (NPs). LS stabilizes and protects the alveolus during its continuous compression and expansion by fine-tuning the surface tension at the air-water interface. Previous modelling studies have reported the biophysical function of LS monolayer and its role, but many open questions regarding the consequences and interactions of airborne nano-sized particles with LS monolayer remain. In spite of gold nanoparticles (AuNPs) having a paramount role in biomedical applications, the understanding of the interactions between bare AuNPs (as pollutants) and LS monolayer components still unresolved. Continuous inhalation of NPs increases the possibility of lung ageing, reducing the normal lung functioning and promoting lung malfunction, and may induce serious lung diseases such as asthma, lung cancer, acute respiratory distress syndrome, and more. Different medical studies have shown that AuNPs can disrupt the routine lung functions of gold miners and promote respiratory diseases. In this work, coarse-grained molecular dynamics simulations are performed to gain an understanding of the interactions between bare AuNPs and LS monolayer components at the nanoscale. In these simulations model, two different surface tensions of the monolayer are used to mimic the biological process of breathing (inhalation and exhalation). It is found that the NP affects the structure and packing of the lipids by disordering lipid tails. Overall, the analysed results suggest that bare AuNPs impede the normal biophysical function of the lung, a finding that has beneficial consequences to the potential development of treatments of various respiratory diseases.

INTRODUCTION

LS is a thin liquid layer inside the alveolus that forms a stable monolayer at the air-water interface and is composed of phospholipids, cholesterol, and proteins. The importance of LS is its function to reduce surface tension during expiration and prevent the lung from collapsing. Secondly, LS also acts as a first biological barrier for all the inhaled pathogens and pollutants. Lipids, cholesterol (neutral lipids), and proteins are the main components of the LS. Notably, lipids, which are the major components of the LS (about 92%) assist to reduce the surface tension nearly to zero during exhalation [1-3]. Dipalmithoylphosphatidycholine (DPPC), which typically makes up half of total surfactant lipid population, plays a significant role in maintaining the surface tension at the interface. During inhalation, the surfactant monolayer expands, but it compresses at the time of exhalation. Surface tension at the interface fluctuates from nearly 0 mN/m [4, 5] to the equilibrium value 20~25 mN/m [5, 6] during the monolayer compression and expansion process respectively.

Structural changes occur in LS monolayers during the inhalation-exhalation cycle, and molecular simulations can predict lipid structural properties at the nanoscale, e.g. phase behaviour, the area per lipid (APL), lipid chain order parameter, and radial distribution function (RDF). Similarly, the dynamical properties can be obtained through the calculation of lipid mean square displacement (MSD), and the lateral diffusion coefficient of lipids. The structural properties of the monolayer is correlated with each other. The monolayer at the air-water interface changes from the liquid expanded (LE) phase to the liquid condensed (LC) phase as the APL decreases. Similarly, the surface tension of the monolayer is directly proportional to the APL [6], and it achieves its highest value in the LE phase and reduces nearly to 0 mN/m in the LC phase. Surface tension can also be reduced to the equilibrium value due to the adsorption of surface-active

substances at the LS interface [7, 8]. The physiological activities of the lung can be hampered in the presence of unexpected pathogens or pollutant nanoparticles in the lung area.

Nanoparticles mainly enter into the respiratory system through the nasal cavity, pass the trachea region and then reach in the lower lung. The nanoparticles (<100 nm) can travel further down to alveolus region where gas exchange happens. These ultrafine NPs are considered most harmful [9-11] and can create many health hazards particularly in the lungs. Inside the alveolus, the nanoparticles are trapped by the surfactant layer. The nanoparticles affect different surfactant structural and dynamical properties when they interact with the surfactant components. Such changes in LS monolayer properties could disrupt the normal function of the lung, and the disruption may induce many lung diseases including lung cancer, asthma, respiratory distress syndrome and more [9, 12].

Research on NPs either engineered (prepared in the laboratory for drug delivery) or environmental (as pollutants) with surfactant monolayer have explored the potential use of the NPs as therapeutic agents as well as the causes and consequences of the NPs inhalation from the environment. Researchers have shown considerable interest in the use of gold NPs (AuNPs) because AuNPs can be synthesized into various sizes, shapes, and their surface can be modified by attaching bioactive molecules or chemical functionalized groups [13-16]. The engineered AuNPs can be a therapeutic and diagnostic agent for cancer by targeting tumour cells [17]. Like other NPs [18-21], bare AuNPs (engineered or environmental) can alter the surfactant structural and dynamical properties. Experimentally it has been shown that bare AuNPs can disrupt the normal lung function by impeding the ability to lower the surface tension values during alveolus compression [15, 16].

The permeation of environmental and engineered bare AuNP through the LS monolayer have not studied before. Therefore the molecular-level understanding on AuNP translocation and permeation into the LS is still not properly understood. MD simulations have been performed to understand these interactions among LS monolayer components and AuNP. To the best of our knowledge, modelling of the interactions of bare AuNP with LS monolayer has not been reported previously. This study will help to understand the biophysics of NP penetration into LS monolayer. The molecular-level information on the interaction mechanism between AuNP and LS components that obtained through our simulations will offer a new way of thinking about the effects of AuNP on the behaviour on LS during breathing.

MODEL AND METHOD

The initial LS system was built using an INSANE [22] script and consisted of a mixture of DPPC and POPG phospholipids (7:3) lipids. The INSANE script produced a bilayer with a dimension 25×25 nm^2 and the two monolayers were prepared by splitting the bilayer about 6 nm. Then the 6 nm gap was filled by ~26000 CG water beads, resulting in a density of ~1 kg/L. The monolayer (in *xy*-plane) on each side of the water layer contained 1023 CG lipids molecules (716 DPPC and 307 POPG). In the presence of water, lipids are oriented its tails towards the air and polar heads towards the water. To counteract the presence of the negatively charged POPG lipid, a number of -water beads, such as to ensure the system was charge neutral, were replaced by positive CG ions (NA+). All the lipids, water and ions were placed in a cubic periodic box of dimension 25×25×60 nm^3, such that the lipid monolayers were separated by approximately 40 nm of vacuum, (Figure 1). The initial system was prepared using a similar procedure as described by Estrada-López *et al.* [23]. In addition to the control (monolayer+water) systems, simulations were also performed on systems containing a 3 nm (diameter) bare AuNP wherein, the NP was placed in the vacuum about 6 nm above one monolayer, in order to represent the LS monolayer in the presence of a pollutant. The difference in the systems with and without AuNP may contribute to predict the influence of pollutants in LS during inhalation and exhalation.

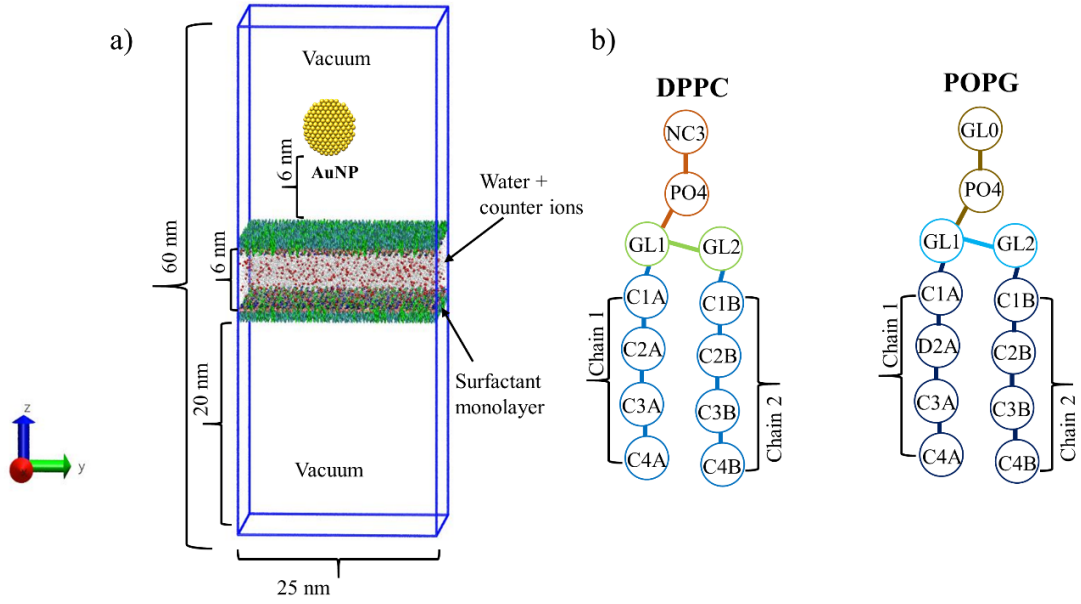

Figure 1. (a) Simulation system configuration with the two lipid monolayers separated by 6 nm water/40 nm vacuum, the AuNP were placed in vacuum ~6 nm from a monolayer, (b) schematic representation the coarse-grained lipid models (DPPC and POPG), with MARTINI bead type.

GROMACS version 5.1.4 [24] was used to perform all the simulations. All the necessary input parameters for lipids, ions, and water were taken from MARTINI websites [25]. MARTINI C5-type interaction site was assigned for each Au bead as described by Song *et al*. [26]. OpenMD [27] was used to construct the atomistic structure of an AuNP of diameter 3 nm with a lattice constant 0.408 nm. The final AuNP consisted of 887 atoms, and each atom was mapped 1:1 into CG Au bead. Harmonic bonds were applied to connect all AuNP beads in accordance with previous studies [28, 29].

Before simulation, all systems were energy minimized using the steepest descent algorithm to avoid all the unrealistic interactions among lipids, water, and ions molecules. Periodic boundary conditions (PBC) were applied in all directions. Coulomb interactions the cutoffs were shifted to 0 and 1.2 nm, but for the Lennard-Jones interactions, the cutoffs value 0.9 and 1.2 nm were considered for equilibration and production run. In all simulations, lipids, water, and ions molecules were coupled separately at 310K using v-rescale thermostat [30] (close to the phase transition temperature of DPPC). Simulations were performed on systems with and without the AuNP present at two surface tensions 0 and 23 mN/m, corresponding to the compression and expansion states, respectively, for a total of four systems simulated. The equilibration and production simulations were performed in the NPγT (constant particle number, pressure and temperature) ensemble at surface tensions 0 mN/m and 23 mN/m using Berendsen pressure coupling [31] with 4.5×10^5 bar^{-1} compressibility in the *xy*-plane. All the systems were considered 100 ns equilibration and 3 μs production run with 20 fs time step. The box height was kept constant in the normal direction to the monolayer plane by setting the compressibility to 0 bar^{-1}.

The Visual Molecular Dynamics (VMD) program [32] was used to render the snapshots. Analyses of the order parameter, density profiles, and RDF were carried out over the last 1 μs of each system. The lipid order parameter was calculated using the following formula

$$S_{CD} = \frac{1}{2}(3 < \cos^2\theta > -1) \qquad (1)$$

where θ is the angle between lipid tail beads and monolayer normal. $S_{CD} = 0$ indicates a random (isotropic) orientation of the tails, $S_{CD} = 1$ defines that the lipid tails are in perfect alignment and $S_{CD} = -0.5$ for perfect anti-alignment of the tails.

RESULTS AND DISCUSSION

Comparison of the four systems simulated with and without the presence of an AuNP and at surface tensions of 0 and 23 mN/m allowed the changes in the structural properties of the LS monolayer during inhalation and exhalation to be predicted. The APL values of the different systems are given in Table I. The data indicate that the presence of the AuNP has a negligible effect on the average APL values of the surfactant monolayer, with the surface tension being the factor controlling the APL. The APL values predicted good agreement with the experimental [16] and published results [23] where ~15% reduction in APL reported during monolayer compression from the expansion state. The APL values ~0.47-0.49 nm^2 indicate that the surfactant lipid monolayer exist in liquid condensed phase (LC) [33]. In our simulations, the LC phase was attained during compression process of LS monolayer at surface tension 0 mN/m.

Table I. APL of the surfactant monolayer obtained at two different surface tensions 0 mN/m and 23 mN/m, the surface tensions during exhalation and inhalation state respectively.

System	Surface Tension (mN/m)	APL (Å)
DPPC, POPG	0	47.43±0.04
	23	57.12±0.08
DPPC, POPG, AuNP	0	46.19±0.05
	23	57.03±0.08

The obtained APL values at surface tension 23 mN/m postulate that the surfactant monolayer attained the coexistence of liquid condensed-expanded phase. In the LC phase, lipids were found very tightly packed and more ordered in comparison with the lipids at surface tension 23 mN/m (inhalation state). To quantify this, we computed the order parameter of the lipid tails chain 1 (sn-1) and chain 2 (sn-2). The order parameter of lipids provides information on the structural orientation and ordering of lipids in the monolayer. The unsaturated lipid, POPG (with a double bond in chain 1) was more disordered than the saturated lipid DPPC at both surface tensions (Figure 2). In the absence of the AuNP, the phospholipids were more ordered at low surface tension than high surface tension. But, the presence of AuNP in the monolayer induced a switch with the phospholipid tails more ordered at surface tension 23 mN/m than at surface tension 0 mN/m. This change occurred in both the *sn*-1 and *sn*-2 chains. The change in lipid order parameter signifies that AuNP disordered the normal lipid packing and may lead disruption in surfactant monolayer.

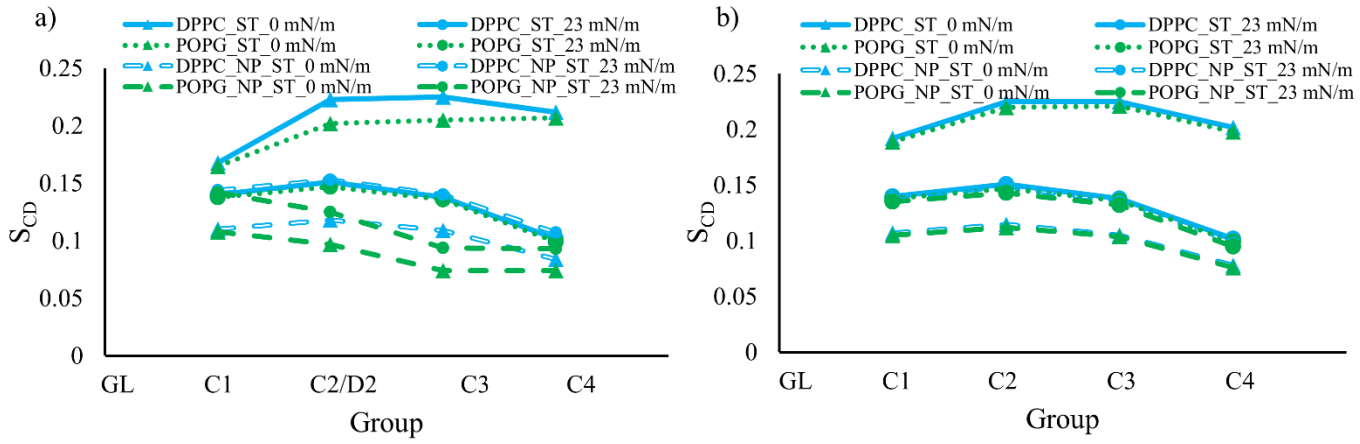

Figure 2. Order parameters for DPPC (simple and double solid blue lines) and POPG (round dot and dash green lines) chain beads (a) chain 1 (sn-1) and (b) chain 2 (sn-2) at two different surface tensions 0 mN/m (lines with triangular marker) and 23 mN/m (lines with circular marker). The simple solid and dot lines represent the system without AuNP and double solid and dash lines represent the system with AuNP.

Single AuNP marginally affected the APL values of LS monolayer at both surface tensions (Table I) but significantly changed the order parameter values (Figure 2). However, the snapshots of the lipid monolayer in the presence of AuNP at surface tension 0 mN/m (Figure 3a) and 23 mN/m (Figure 3b) indicate that AuNP strongly interacted with the monolayer lipids at surface tension 0 mN/m (Figure 3a). The interaction created a rupture in the monolayer at low surface tension while such change was not found in the monolayer at surface tension 23 mN/m (Figure 3b). As a result of the disruption during compression, the lipids in the monolayer and water density profiles (Figure 3c) were dropped from their physiological values. During monolayer expansion, a single AuNP showed negligible effects in lipids and water densities (Figure 3d). The snapshots (Figure 3a and b) also demonstrate that the AuNP absorbed on the monolayer surface quickly and interacted with the surfactant components (Figure 3a and b). During the interactions between the AuNP and the LS components, the LS lipids wrapped the AuNP.

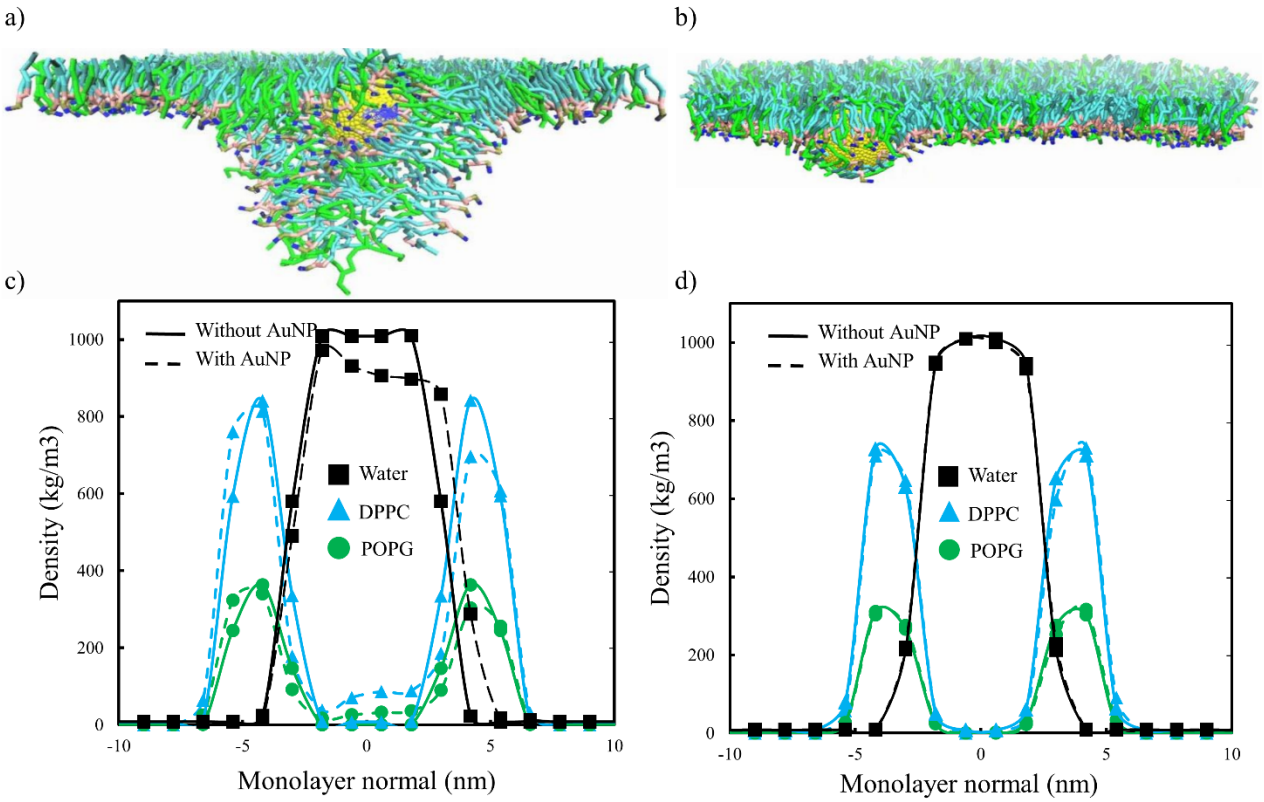

Figure 3. (a) The snapshot of AuNP interactions with LS lipids (side view) at surface tensions (a) 0 mN/m and (b) 23 mN/m. Density profiles of DPPC (lines with triangular marker), POPG (lines with circular marker), and water (lines with square marker) were calculated for the system with AuNP (dash lines) and without AuNP (solid) at surface tensions (c) 0 mN/m and (d) 23 mN/m.

Au beads were considered as hydrophobic (C5 type) using the Martini force fields. Therefore, the hydrophobic tail beads presumably interact strongly with the Au beads under both inhalation and exhalation. To quantify this, we calculated the integral of RDF (coordination number) of lipids tail and head beads around the Au beads at surface tensions 0 mN/m (Figure 4a) and 23 mN/m (Figure 4b). The coordination number allows measuring the number of lipid beads around the AuNP beads. The integral was taken to the first minimum of the RDF. Figure 4 shows that the coordination number of lipid tail beads were higher than the lipid head beads.

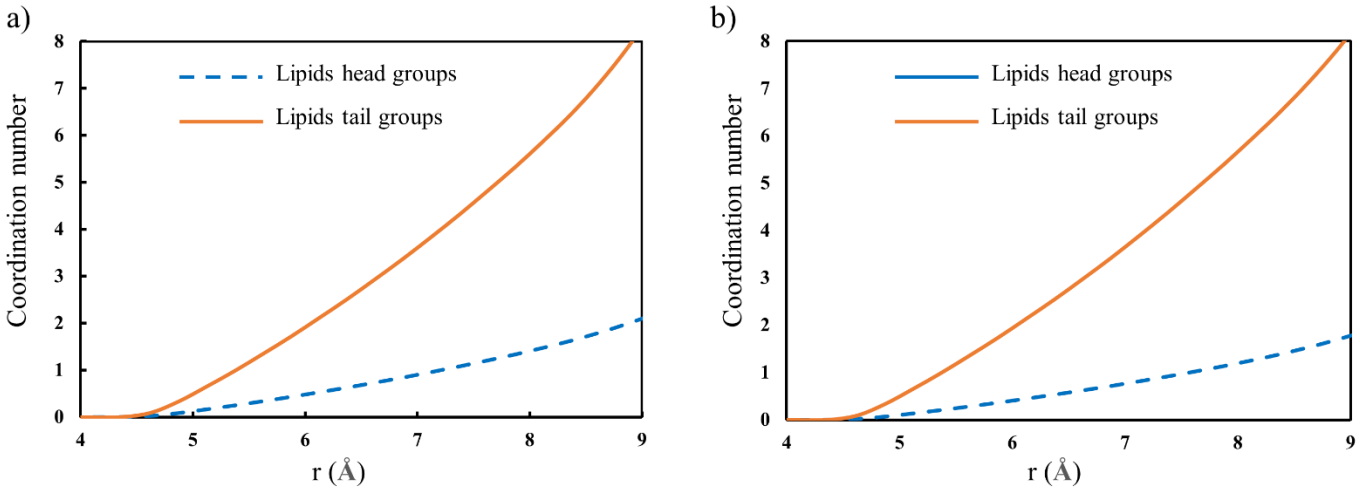

Figure 4. (a) Integral of RDFs (coordination number) between Au beads and head beads (dash line) and tail beads (solid line) of surfactant lipids were calculated at surface tension (a) 0 mN/m (b) 23 mN/m.

In the monolayer, if there are no restricted interactions among the heterogeneous lipids, then lipids can freely move laterally in the monolayer. To monitor this effect, the lateral diffusion coefficients of the heterogeneous system (DPPC and POPG lipid monolayer) were calculated. The results for each monolayer are presented in Table II. Both surfactant lipids species (DPPC and POPG) diffused laterally, with similar rates at both surface tensions.

The absence of AuNP in the systems, lateral diffusion coefficients of DPPC and POPG at surface tension 0 mN/m were increased almost seven fold at surface tension at 23mN/m. During exhalation, i.e. at low surface tension, the lipid monolayer becomes compressed and gives low diffusion of monolayer lipids. On the other hand, at high surface tension, i.e., during inhalation monolayer lipids get more space to diffuse and result in high diffusion. Here, at the surface tension 0 mN/m, the diffusion of surfactant phospholipids in a system without AuNP were about three times less than their diffusion in a system with AuNP due to the significant disruption in the monolayer by the AuNP. In summary, the lipids diffusion enhanced during monolayer expansion than compression process and single AuNP had less influence on the lipids diffusion in the monolayer expansion state.

Table II. Lateral diffusion coefficients of DPPC and POPG at 0 mN/m and 23 mN/m in the presence and absence of AuNP in the surfactant monolayer.

System	Lipid Molecules	Surface Tension (mN/m)	Lateral Diffusion Coefficient, D (10^{-7} cm^2s^{-1})
DPPC,POPG	DPPC	0	1.15 ± 0.30
	POPG		1.24 ± 0.32
	DPPC	23	8.76 ± 0.01
	POPG		8.73 ± 0.01
DPPC,POPG,NP	DPPC	0	3.53 ± 0.28
	POPG		3.53 ± 0.28
	DPPC	23	8.42 ± 0.01
	POPG		8.29 ± 0.04

CONCLUSIONS

We have studied the effect of AuNP on the LS monolayer at two different surface tensions 0 mN/m and 23 mN/m using coarse-grained molecular dynamics simulation. These two surface tensions represent surfactant monolayer compression and expansion states. As a pollutant, the AuNP affected the structure and dynamical properties of the surfactant lipids at both surface tensions. AuNP can alter the lipid packing, change the physiological densities of lipids and water and more importantly it can accelerate the lipid lateral diffusion. All these changes were mostly observed at low surface tension. Therefore, single bare AuNP had less influence on surfactant monolayer components and their biophysical properties at high surface tension. It was also observed that the hydrophobic AuNP beads were profoundly attracted by the hydrophobic lipid tails beads. In this study, we used single AuNP only at upper monolayer. It implies that a very low concentration of Au was used. Higher concentration of bare AuNP may lower the normal lung function ability. However, the causes and consequences that observed in the surfactant monolayer due to single AuNP permeation cannot be overlooked. The hypothesis

of this study suggests that during monolayer compression AuNP has a broader impact than monolayer expansion. The outcome of this study will assist to understand the causes and consequences of NP inhalation, as well as the coarse-grained model of LS lipids and AuNP, may be beneficial to design future nanomedicine for lung diseases.

ACKNOWLEDGMENTS

This study was supported by the University of Technology Sydney (UTS) FEIT Research Scholarship, 2018 Blue Sky scheme–Suvash Saha (Activity 2232368), and N.S.G is supported by the Vice-Chancellor fellowship funded by QUT. The resources were provided by the UTS HPC services, QUT HPC and, NCI Australia.

REFERENCES

1. R. Veldhuizen, K. Nag, S. Orgeig and F. Possmayer, *Biochim. Biophys. Acta-Mol. Basis Dis.*, **1408**, 90-108 (1998).
2. S. Rugonyi, S. C. Biswas and S. B. Hall, *Respir. Physiol. Neurobiol.*, **163**, 244-255 (2008).
3. H. Zhang, Y. E. Wang, Q. Fan and Y. Y. Zuo, *Langmuir*, **27**, 8351-8358 (2011).
4. E. Lopez-Rodriguez and J. Perez-Gil, *Biochim. Biophys. Acta-Biomembr.*, **1838**, 1568-1585 (2014).
5. A. Fathi-Azarbayjani and A. Jouyban, *BioImpacts*, **5**, 29-44 (2015).
6. S. Schürch, F. H. Y. Green and H. Bachofen, *Biochim. Biophys. Acta-Mol. Basis Dis.*, **1408**, 180-202 (1998).
7. V. Ponec, *Recl. Trav. Chim. Pays-Bas*, **110**, 137-137 (1991).
8. G. L. Gaines, *Insoluble monolayers at liquid-gas interfaces*, (Interscience Publishers, 1966).
9. N. Li, M. Hao, R. F. Phalen, W. C. Hinds and A. E. Nel, *Clin. Immunol.*, **109**, 250-265 (2003).
10. J. W. Anseth, A. J. Goffin, G. G. Fuller, A. J. Ghio, P. N. Kao and D. Upadhyay, *Am. J. Respir. Cell Mol. Biol.*, **33**, 161-168 (2005).
11. C. Sioutas, R. J. Delfino and M. Singh, *Environ. Health Perspect.*, **113**, 947-955 (2005).
12. I. C. Pope, R. T. Burnett, M. J. Thun and et al., *JAMA*, **287**, 1132-1141 (2002).
13. D. B. Sridhar, R. Gupta and B. Rai, *Phys. Chem. Chem. Phys.*, **20**, 25883-25891 (2018).
14. G. Rossi and L. Monticelli, *Biochim. Biophys. Acta, Biomembr.*, **1858**, 2380-2389 (2016).
15. K. Zhang, L. Liu, T. Bai and Z. Guo, *J. Biomed. Nanotechnol.*, **14**, 526-535 (2018).
16. M. S. Bakshi, L. Zhao, R. Smith, F. Possmayer and N. O. Petersen, *Biophys. J.*, **94**, 855-868 (2008).
17. I. H. El-Sayed, X. Huang and M. A. El-Sayed, *Nano Lett.*, **5**, 829-834 (2005).
18. J. Barnoud, L. Urbini and L. Monticelli, *J. Royal Soc. Interface*, 2015, **12**.
19. T. Yue, Y. Xu, S. Li, Z. Luo, X. Zhang and F. Huang, *RSC Adv.*, **7**, 20851-20864 (2017).
20. R. P. Valle, T. Wu and Y. Y. Zuo, *ACS Nano*, **9**, 5413-5421 (2015).
21. Q. Hu, B. Jiao, X. Shi, R. P. Valle, Y. Y. Zuo and G. Hu, *Nanoscale*, **7**, 18025-18029 (2015).
22. T. A. Wassenaar, H. I. Ingolfsson, R. A. Bockmann, D. P. Tieleman and S. J. Marrink, *J. Chem. Theory Comput.*, **11**, 2144-2155 (2015).
23. E. D. Estrada-Lopez, E. Murce, M. P. P. Franca and A. S. Pimentel, *RSC Adv.*, **7**, 5272-5281 (2017).
24. M. J. Abraham, T. Murtola, R. Schulz, S. Páll, J. C. Smith, B. Hess and E. Lindahl, *SoftwareX*, **1–2**, 19-25 (2015).
25. Martini-Coarse Grain Forcefield for Biomolecules. Available at:http://cgmartini.nl/index.php (assessed 10 April 2018)
26. B. Song, H. Yuan, C. J. Jameson and S. Murad, *Mol. Phys.*, **110**, 2181-2195 (2012).
27. Gezelter, J. D.; Kuang, S.; Marr, J.; Stocker, K.; Li, C.; Vardeman, C. F.; Lin, T.; Fennell, C. J.; Sun, X.; Daily, K.; Zheng, Y. OpenMD, an Open Source Engine for Molecular Dynamics, Available at:http://openmd.org/ (accessed 21 April 2017)
28. O. Lopez-Acevedo, J. Akola, R. L. Whetten, H. Grönbeck and H. Häkkinen, *J. Phys. Chem. C*, **113**, 5035-5038 (2009).
29. S. Salassi, F. Simonelli, D. Bochicchio, R. Ferrando and G. Rossi, *J. Phys. Chem. C*, **121**, 10927-10935 (2017)
30. G. Bussi, D. Donadio and M. Parrinello, *J. Chem. Phys.*, **126**, 014101 (2007).
31. H. J. C. Berendsen, J. P. M. Postma, W. F. van Gunsteren, A. DiNola, and J. R. Haak, *J. Chem. Phys.*, **81**, 3684-3690 (1984).
32. W. Humphrey, A. Dalke and K. Schulten, *J Mol Graph*, **14**, 33-38 (1996).
33. S. Baoukina, L. Monticelli, S. J. Marrink and D. P. Tieleman, *Langmuir*, **23**, 12617-12623 (2007).